Research Article

Multiphase calcium alginate membrane composited with cellulose nanofibers for selective mass transfer

Ryo-ichi Nakayama[1] · Yusuke Takamatsu[1] · Norikazu Namiki[1]

Abstract

A multiphase calcium alginate membrane composited with cellulose nanofibers (CNF) was successfully prepared by using the method. The maximum stress and strain, water content, water permeability, and mass transfer characteristics were examined according to the addition ratio of CNF. Increasing of the amount of CNF enhanced the maximum stress and reduced the maximum strain, thereby suggesting that CNF impart flexibility and stiffness to the composite membrane. The CNF in the calcium alginate noticeably increased the water flux at the same pressure. The permeability of the composite of the CNF membrane was higher. The effective diffusion coefficient dramatically decreased 2.5×10^3 times when the molecular weight increased ten-fold (from 60 to 604 Da). Moreover, stronger dependency was observed in the CNF composite membrane. The morphology of the cross-section of the membrane was observed using scanning electron microscopy. The appearance of the CNF composite membrane became rougher when the amount of CNF increased.

Keywords Cellulose nanofiber · Membrane · Mechanical strength · Effective diffusion coefficient · Water permeability

List of symbols

A_c	Initial membrane cross-sectional area (m^2)
A_m	Effective area of the membrane (m^2)
B_{max}	Maximum breaking load (N)
C_{fi}	Initial concentration in the feed solution (mol/L)
C_s	Concentration in the stripping solution (mol/L)
D	Diffusion coefficient estimated from an empirical equation in the bulk aqueous phase (m^2 s^{-1})
D_{eff}	Effective diffusion coefficient (m^2 s^{-1})
d	Diameter of glass petri dish (m)
H_V	Volumetric water content of membrane, defined by Eq. (4) (–)
J_V	Volumetric water flux (m$^3_{water}$ m$^{-2}_{area}$ s^{-1})
K_{OL}	Overall mass transfer coefficient (m s^{-1})
k_m	Membrane mass transfer coefficient (m s^{-1})
L	Length of membrane at break (m)
L_i	Initial length of membrane (m)
L_p	Water permeability coefficient (m$^3_{water}$ m$^{-2}_{area}$ m$^{-1}_{thickness}$ Pa^{-1} s^{-1})
l_m	Membrane thickness (m)
M	Molar mass of solvent (g mol^{-1})
P	Operational pressure (Pa)
R_{CNF}	Additional rate of CNF (%)
T	Temperature (K)
t	Mass transfer operation time (s)
V	Volume of aqueous solution in transfer cell (m^3)
V_p	Volumetric amount of permeated water (m^3)

Greek symbols

δ	Maximum stress (Pa)
ε	Void fraction of membrane, estimated from volumetric water content H_v (–)
λ	Maximum strain (%)
μ	Viscosity of solvent (Pa s)
v	Molar volume of solute at boiling point (m^3 mol^{-1})
Π	Osmotic pressure difference (Pa)
σ	Reflection coefficient of solute (–)
τ	Tortuosity of membrane (–)
φ	Association factor for solvent in Eq. (9) (–)

✉ Ryo-ichi Nakayama, bionakayama.ryo@cc.kogakuin.ac.jp | [1]Department of Environmental Chemistry and Chemical Engineering, School of Advanced Engineering, Kogakuin University, 2665-1 Nakano-machi, Hachioji, Tokyo 192-0015, Japan.

1 Introduction

Membrane separation processes are attractive because of their low energy cost as well as their ability to deliver contaminant-free final product [1–3]. Recently, interest in using natural materials for membranes has increased because of their biocompatibility and environmentally friendly disposability. The success of synthetic biopolymers can be attributed to their wide range of mechanical properties and the development of transformation processes that allow a variety of different shapes to be easily produced inexpensively as well as their good biocompatibility [4–6].

Sodium alginate is a biopolymer that can be possibly used as an environmentally compatible material for medical, food, and industrial applications. It can be sustainably and easily produced from kelp, which is cultivated in oceans worldwide [7–9].

The ability of sodium alginate to form gels with the aid of metal ion exchange (ex. Ca^{2+}) has been extensively applied to form gel particles and membranes [10–12]. The molecular size of the alginate chain is generally not controlled because it is a natural biological product. To improve biopolymer characterization, using a multiphase composite material from a plural biopolymer showed potential to be a promising approach to prepare a tailor-made membrane.

Cellulose is used to produce potential reinforcing bionanomaterials called cellulose nanofibers (CNF) [13–15]. CNF have been researched for their use in biodegradable packaging because they are renewable, narrow diameter, and high mechanical strength [16–18]. Additionally, they have the potential to be used as agents in transparent composites, polymer hybrid-gels, and flexible conductive composites [19, 20]. Interest in the fabrication of films using CNF exists because they have the ability to form a cross-linked network in a very dilute aqueous suspension. All these important characteristics have made CNF an attractive candidate in the field of nanomaterial research. Recently, membranes composited with cellulose nanofibers have gained considerable attention because is a naturally occurring material that has intrinsic and structural advantages such as excellent mechanical properties and hydrophilicity. However, to the best of the authors' knowledge, composited membranes composited with cellulose nanofibers was not previously investigated for selective mass transfer. Using biopolymer-based composite membranes contributes to a more sustainable society. Cellulose nanofibers are compatible with multiphase calcium alginate membrane due to their structural similarity. Thus, their composites are expected to have the physicochemical properties of

alginate acid and the mechanical properties of cellulose nanofibers.

In this study, the authors examined the mechanical strength and mass transfer characteristics of a multiphase composite membrane that was prepared using calcium alginate based biopolymer membranes composited with CNF.

2 Experiments

2.1 Materials

Sodium alginate, calcium chloride, urea, glucose, methyl orange, and Bordeaux S were purchased from Wako Pure Chemical Industries, Ltd. (Osaka, Japan). Cellulose nanofibers were purchased from Sugino Machine, Ltd. (Toyama, Japan).

2.2 Methods

2.2.1 Preparation of calcium alginate membrane composted with cellulose nanofibers

An aqueous solution of sodium alginate (10 g/L) was prepared using distilled water, and a desirable amount of CNF was added to this solution. The mixed solution (20 mL) was poured into a glass petri dish (d = 8.3 cm) and then dried in a thermally controlled oven chamber regulated at 333 K for 12 h. The dried sodium alginate with composite CNF from the petri dish was then immersed in a 0.1 mol/L $CaCl_2$ solution (25 mL) to cross link the alginate polymer chain. After 20 min at room temperature (T = 298 K), the membrane was separated from the glass dish. Subsequently, it was washed with distilled water to remove excess metal ions. The additional rate of CNF, R_{CNF} (%), was evaluated by Eq. (1). In this study, calcium alginate membranes were prepared with the following ratios of cellulose nanofibers: 0%, 5%, 10, 15%, and 20%.

$$R_{CNF} = \frac{Cellulose\ nanofiber\ (g)}{Sodium\ alginate\ (g)} \times 100 \qquad (1)$$

2.2.2 Scanning electron microscopy

The membranes were snap-frozen in liquid nitrogen then dried in a vacuum-freeze dryer (RLE-103, Kyowa Vacuum Engineering. Co., Ltd., Tokyo, Japan) at 298 K for 24 h. The membranes were then sputter-coated using a thin Pt-membrane on a sputter-coater (E-1010 Ion Sputter, Hitachi, Ltd., Tokyo, Japan). Images of the membrane cross sections were obtained using a scanning electron

microscope (SEM, Miniscope TM-1000, Hitachi, Ltd., Tokyo, Japan).

2.2.3 Mechanical strength of the membrane

The mechanical strength of swollen membranes was measured using a rheometer (CR-DX500, Sun Scientific Co., Ltd., Tokyo, Japan). The swollen membrane was cut into sample pieces (1 cm × 4 cm) that were stretched at a speed of 1 mm s^{-1}. These tests were replicated three times. The maximum stress, δ (Pa), and the maximum strain, λ (%), at membrane rupture were calculated using Eqs. (2) and (3).

$$\delta = \frac{B_{max}}{A_c} \tag{2}$$

$$\lambda = \frac{L - L_i}{L_i} \times 100 \tag{3}$$

where B_{max} (N) is the load at membrane rupture, A_c (m^2) is the initial membrane cross-sectional area, L_i (m) is the initial length of the membrane and L (m) is length of the membrane at break.

2.2.4 Volumetric water content

To determine the inner structure of the swollen membrane, analysis was conducted by estimating the volumetric water content from the water content of the membrane. The swollen membrane was cut into squares (4 cm × 4 cm) and contained water in its void spaces. Therefore, volumetric water content was reasonably equivalent to the void fraction in the swollen-state membrane. Excess water on the surface was removed using filter paper, followed by drying in a thermally-controlled oven at 333 K for 24 h. Water loss was gravimetrically measured using an electronic balance. These tests were replicated three times. Volumetric water content was obtained by recalculating the gravimetric change in the membrane. The volumetric water content in the swollen membrane, H_v (–), was estimated by Eq. (4).

$$H_V = \frac{V_w}{V_m} \tag{4}$$

where V_w is the volume of water in the membrane, and V_m is the volume of the swollen membrane.

2.2.5 Water permeation flux

The water permeability of the membrane was determined using an ultra-filtration apparatus (UHP-62K, Advantec Tokyo Kaisha, Ltd., Tokyo, Japan) [21]. The water

permeability area of the membrane was estimated by the ultra-filtration apparatus to be 2.21×10^{-3} m^2. The initial volume of distilled water was constant at 190 mL. The mass of permeated water with running time was measured by an electric balance, and the volume of permeated water was obtained by recalculation using the density of water. Pressure was applied using nitrogen gas introduced from a cylinder. These tests were replicated three times. The water permeation flux, J_v, was measured at 298 K and was defined by Eq. (5).

$$J_V = \frac{V_p}{A_m \cdot t} \tag{5}$$

where V_p is the volume of permeated water, A_m is the membrane surface area, and t is the operating time.

2.2.6 Mass transfer characterization

The mass transfer characterization of the membrane was evaluated from the effective diffusion coefficient of target components. Mass transfer cells were made by sandwiching the examined membranes between two pieces of glass. Aqueous solutions containing each of the target components and stripping water, of the same volume (190 mL), were fed into each cell. Urea (60 Da), d-glucose (180 Da), methyl orange (327 Da), and Bordeaux S (604 Da) were employed as the target components. The aqueous phase was stirred thoroughly (above 850 min^{-1}) to ignore film mass transfer resistance. Under this condition, the overall mass transfer coefficient K_{OL} is the directly the mass transfer coefficient. It was calculated using Eq. (6). Effective diffusion coefficient, D_{eff} (m^2 s^{-1}) was evaluated by Eqs. (7) and (8).

$$\ln\left(1 - \frac{2C_s}{C_{fi}}\right) = -2\frac{A_m}{V} \cdot K_{OL} \cdot t \tag{6}$$

$$K_{OL} = k_m \tag{7}$$

$$k_m = \frac{D_{eff}}{l_m} \tag{8}$$

For comparison, the diffusion coefficient in bulk solvent, D (m^2 s^{-1}) was estimated according to the Wilke–Chang equation.

$$D = 1.86 \times 10^{-18} \frac{(\varphi M)^{0.5} T}{\mu v^{0.6}} \tag{9}$$

where M is the molar mass of the solvent, v is the molar volume of the solute at the boiling point, μ is the viscosity of the solvent, and φ is the association factor for the

solvent at the required temperature T. The value of φ is 2.6 for water.

In this study, tortuosity was calculated using the following equations as diffusion models.

$$D_{eff} = \frac{D \cdot \varepsilon}{\tau} \tag{10}$$

$$\tau = \frac{D \cdot H_V}{D_{eff}} \tag{11}$$

where τ is the tortuosity of the membrane, and ε is the void fraction. Because H_V was assumed to be the void fraction ε of the swollen membrane, it was substituted in Eq. (11).

3 Results and Discussion

3.1 Morphology of the CNF composite membranes

Figure 1 shows images of the CNF composite membranes. A stable CNF composite membrane ($R_{CNF}=20\%$) was successfully prepared using this method. The membrane without CNF ($R_{CNF}=0\%$) was transparent. The CNF appeared to be well dispersed in the composite membrane [22].

Scanning electron microscope images of the cross-sectional morphology showed good dispersion and a tightly spaced structure in the calcium alginate membrane. In the case of the CNF composite membrane, uniform morphology was observed with small flakes appearing as dots that had a tendency to accumulate on the membrane. The appearance of the CNF composite membrane became rougher as the amount of CNF was increased. It speculated that the dense structure of the membranes is attributed to their rigid hydrogen-bonded network and high crystallinity.

3.2 Mechanical strength

Figure 2 shows the value of maximum stress and maximum strain at break of the membrane. The maximum stress gradually increased when the amount of CNF was increased. In contrast, the maximum strain at membrane rupture reduced. In general, the maximum stress increases and the maximum strain decreases at break decreases because the amount of cross-linking agent increases. In this study, the stress and strain curve of the nanocomposite membrane indicated the transition from ductile to plastic behavior when the amount of CNF was increased. The lowering of elongation at break is a common trend that is affected by the volume fraction of the added CNF, the dispersion in the matrix, and the interaction between the CNF and the matrix. The maximum stress of an amylopectin membrane increased by incorporation of CNF into the membrane [23]. Likewise, Nanofiber showed the associated structure to form loose, tree-dimensional new works [24].

3.3 Volumetric water content

Figure 3 depicts the relation between the volumetric water content of the membrane and the membrane

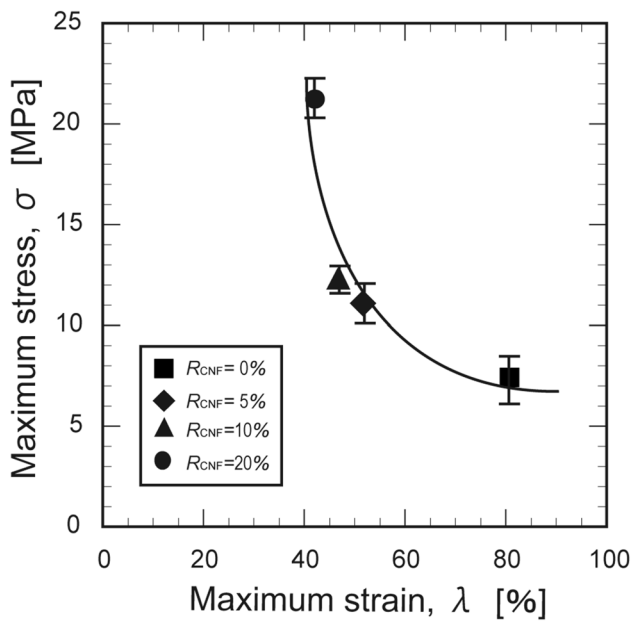**Fig. 1** Scanning electron microscope images of the CNF composite membrane
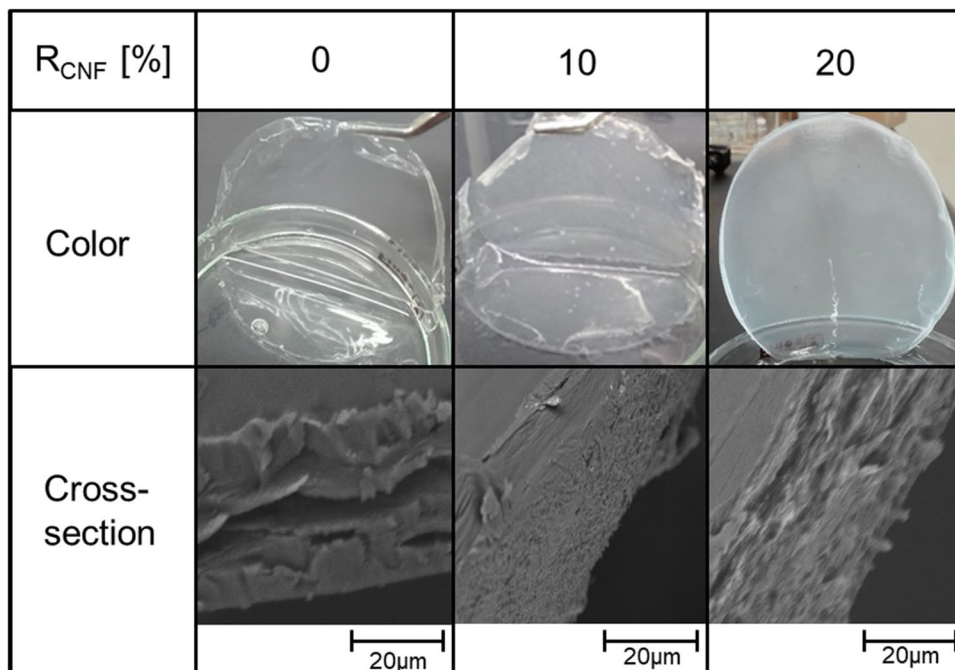
Fig. 2 Change of maximum stress and maximum strain with the CNF composite membrane
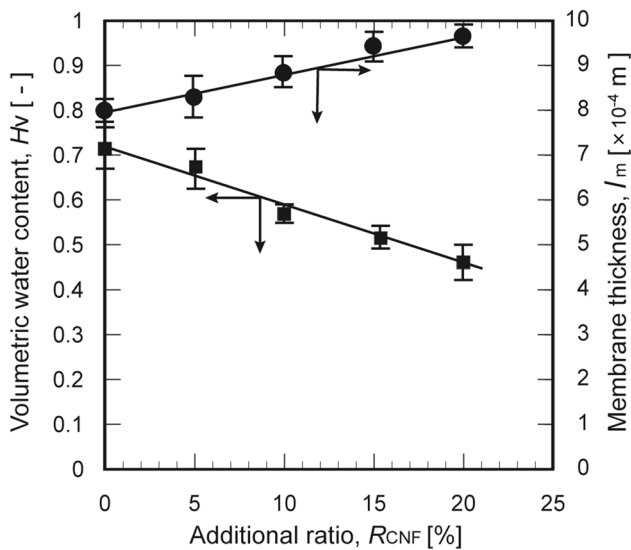

Fig. 3 Effect of CNF on the volumetric water content of calcium alginate membrane and membrane thickness

thickness. H_V decayed linearly and the membrane thickness slightly increased when R_{CNF} increased. The value of H_V reasonably indicated the void fraction in the swollen membrane because the water in the membrane was contained in the voids of the polymer framework of the swollen membrane. The membrane had a greater tendency to not exhibit cellular structures containing free water in void space when the amount of CNF was increased [25].

3.4 Water permeation flux

Figure 4 shows the relation between the water flux and operational pressure acting on the membranes. The water flux of both membranes increased linearly when the operating pressure was increased. The presence of CNF in the calcium alginate membrane noticeably increased the water flux at the same pressure.

This is a commonly observed result in the performance of CNF [26, 27] and is in accordance with Hagen –Poiseuille flow. It can be expressed via non-equilibrium thermodynamic theory using Eq. (10).

$$J_V = L_P(\Delta P - \sigma \Delta \Pi) \tag{12}$$

where L_p (m$^3_{water}$ m$^{-2}_{area}$ Pa^{-1} s^{-1}) is the water permeability coefficient, ΔP is the operational pressure, σ is the reflection coefficient of the solute, and $\Delta \Pi$ is the osmotic pressure difference. When σ equals zero, J_v is linearly proportional to ΔP. The value of L_p of $R_{CNF} = 0\%$ was 2.99×10^{-8}, and that of $R_{CNF} = 20\%$ was 8.13×10^{-9}. The permeability of the composite CNF membrane was higher. The value of L_p for the CNF composite membrane was less than that of a chitosan membrane.

3.5 Mass transfer characterization

The effective diffusion coefficient versus the molecular weight of the tested component has been shown in Fig. 5. The effective diffusion coefficient was logarithmically
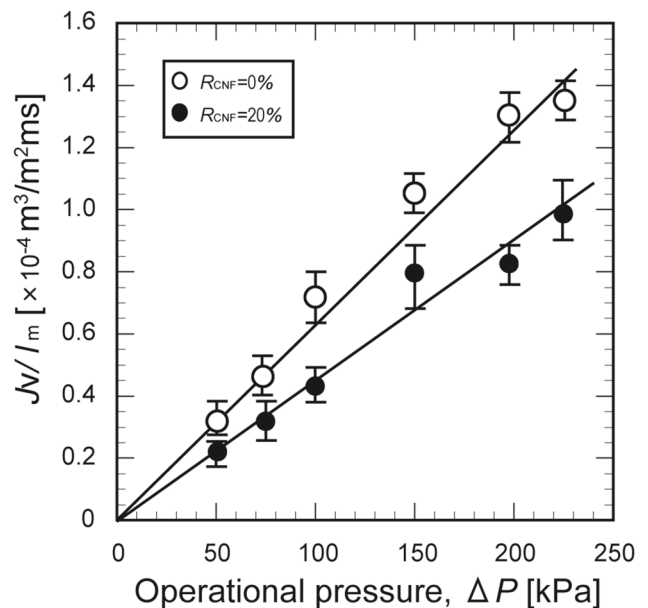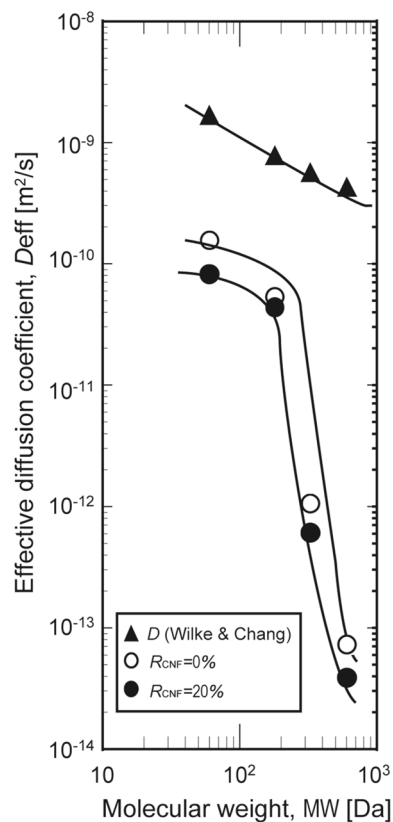

Fig. 4 Volumetric water flux of CNF composite membrane at different pressures
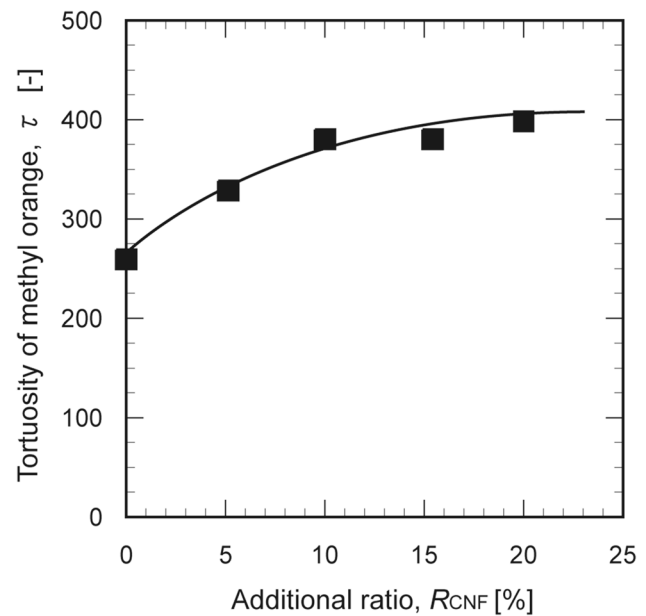
Fig. 5 Effect of molecular weight on the effective diffusion coefficient (D_{eff})

Fig. 6 Effect of the tortuosity on the CNF composite membrane

decayed with increasing molecular weight. These results suggest formation of intermolecular hydrogen bonds between the hydroxyl groups of the cellulose nanofibers and carboxyl groups of the alginate. It is hypothesized that Ca^{2+}/alginate membranes can form in CNF and decrease the membrane pore size.

For the CNF composite membrane, D_{eff} dramatically decreased 2.5×10^3 times when the molecular weight increased 10 times. For the membrane without CNF, D_{eff} decreased 1.7×10^3 times. In contrast, D in the bulk aqueous phase decreased only 3.8 times. This result suggests that the mass transfer channel in the CNF composite membrane was smaller than that in the membrane without CNF. Nomoto and Imai reported a large dependence on molecular size for specific polymer frameworks using a chitosan membrane [28]. Many food ingredients such as amino acids, polyphenols, and saccharides, have a molecular weight within the range tested (60 < MW < 600). Therefore, the CNF composite membrane is expected to be useful for the selective separation of food ingredients.

Figure 6 presents the tortuosity of methyl orange on the amount of CNF in the membrane. The tortuosity of the CNF composite membrane increased when the amount of CNF was increased. This result indicates that the polymeric framework of the membrane was more densely populated when the amount of CNF was increased.

4 Conclusion

A multiphase calcium alginate membrane composited with CNF was successfully prepared using a casting method. The maximum stress gradually increased when the amount of CNF was increased. The CNF composite membrane has sufficient mechanical strength to be repeatedly used. For the CNF composite membrane, D_{eff} dramatically decreased 2.5×10^3 times when the molecular weight increased 10 times. Many functional food ingredients such as sugars, amino acids, and polyphenols are found in this special molecular weight range (60–604 Da). Therefore, high potential exists for the selective separation of glucose using a CNF composite membrane for application in downstream processing in food chemical engineering.

Compliance with ethical standards

References

1. Katsoufidou K, Yiantsios SG, Karabelas AJ (2007) Experimental study of ultrafiltration membrane fouling by sodium alginate and flux recovery by backwashig. J Membr Sci 300:137–146

2. Cao DQ, Hao XD, Wang Z, Song X, Iritani E, Katagiri N (2017) Membrane recovery of alginate in an aqueous solution by the addition of calcium ions: Analyses of resistance reduction and fouling mechanism. J Membr Sci 535:312–321

3. Konca K, Emecen PZC (2019) Effect of carboxylic acid crosslinking of cellulose membranes on nanofiltration performance in ethanol and dimethylsufoxide. J Membr Sci 587:117175

4. Kanti P, Srigowri K, Madhuri J, Smitha B, Sridhar S (2004) Dehydration of ethanol through blend membranes of chitosan and sodium alginate by pervaporation. Sep Purif Technol 40:259–266

5. Wu P, Imai M (2011) Food polymer pullulan-κ-carrageenan composite membrane performed smart function both on mass transfer and molecular size recognition. Desalin Water Treat 34:239–245

6. Dudek G, Turczyn R, Gnus M, Konieczny K (2018) Pervaporative dehydration of ethanol/water mixture through hybrid alginate membranes with ferroferic oxide nanoparticles. Sep Purif Technol 193:398–407

7. Sakai S, Ono T, Ijima H, Kawakami K (2002) Permeability of alginate/sol-gel synthesized aminopropyl-silicate/alginate membrane templated by calcium-alginate gel. J Membr Sci 205:183–189

8. Yadav M, Rhee KY, Park SJ (2014) Synthesis and characterization of graphene oxide/carboxymethyl cellulose/alginate composite blend films. Carbohydr Polym 110:18–25

9. Wang S, Ju J, Wu S, Lin M, Sui K, Xia Y, Tan Y (2020) Electrospinning of biocompatible alginate-based nanofiber membranes via tailoring chain flexibility. Carbohydr Polym 230:115665

10. Nigiz FU, Hilmioglu ND (2013) Pervaporation of ethanol/water mixtures by zeolite filled sodium alginate membrane. Desalin Water Treat 51:637–643

11. Kashima K, Imai M (2017) Selective diffusion of glucose, maltose, and raffinose through calcium alginate membranes characterized by a mass fraction of guluronate. Foof Bioprod Process 102:213–221

12. Nornberg AB, Gehrke VR, Mota HP, Camargo ER (2019) Alginate-cellulose biopolymeric beads as efficient vehicles for encapsulation and slow-release of herbicide. Colloids Surf B 583:123970

13. Siro I, Plackett D (2010) Microfibrillated cellulose and new nano-composite materials: a review. Cellulose 17:459–494

14. Kowalczyk M, Piorkowska E, Kulpinski P, Pracella M (2012) Mechanical and thermal properties of PLA composites with cellulose nanofibers and standard size fibers. Compos A 42:1509–1514

15. Nurani M, Akbari V, Taheri A (2017) Preparation and characterization of metformin surface modified cellulose nanofiber gel and evaluation of its anti-metastatic potentials. Carbohydr Polym 165:322–333

16. Ma H, Burger C, Hsiao BS, Chu B (2014) Fabrication and characterization of cellulose nanofiber based thin-film nanofibrous composite membranes. J Membr Sci 454:272–282

17. Kulpinski P (2005) Cellulose nanofibers prepared by the N-metyl-morpholine-N-oxide method. J Appl Polym Sci 98:1855–1859

18. Abe K, Yano H (2012) Cellulose nanofiber-based hydrogels with high mechanical strength. Cellulose 19:1907–1912

19. Wang Z, Ma H, Hsiao BS, Chu B (2014) Nanofibrous ultrafiltration membranes containing cross-linked poly (ethylene glycol) and cellulose nanofiber composite barrier layer. Polymer 55:366–372

20. Abe K, Yano H (2011) Formation of hydrogels from cellulose nanofibers. Carbohydr Polym 85:733–737

21. Takahashi T, Imai M, Suzuki I (2008) Cellular structure in an N-acetyl-chitosan membrane regulate water permeability. Biochem Eng J 42: 20–27. J Chitin Chitosan Sci 2:1–8

22. Chen C, Mo M, Chen W, Pan M, Xu Z, Wang H, Li D (2018) Highly conductive nanocomposites based on cellulose nanofiber networks via NaOH treatments. Compos Sci Technol 156:103–108

23. Peng X, Ren J, Zhong L, Sun R (2011) Nanocomposite films based on xylan-rich hemicelluloses and cellulose nanofibers with enhanced mechanical properties. Biomacromol 12:3321–3329

24. Soni B, Hassan EB, Schilling MW, Mahmoud B (2016) Transparent bionanocomposite films based on chitosan and TEMPO-oxidized cellulose nanofibers with enhanced mechanical and barrier properties. Carbohydr Polym 151:779–789

25. Hartman J, Albertsson AC, Lindblad MS, Sjoeberg J (2006) Oxygen barrier materials from renewable sources: material properties of softwood hemicellulose-based films. J Appl Polym Sci 100:2985–2991

26. Shao LL, An QF, Ji YL, Zhao Q, Wang XS, Zhu BK, Gao CJ (2014) Preparation and characterization of sulfated carboxymethyl cellulose nanofiltration membranes with improved water permeability. Desalination 338:74–83

27. Jang W, Park Y, Park C, Seo Y, Kim JH, Hou J, Byun H (2020) Regulating the integrity of diverse composite nanofiber membranes using an organoclay. J Membr Sci 15:117670

28. Nomoto R, Imai M (2013) Dominant Role of Acid-Base Neutralization Process in Forming Chitosan Membranes for Regulating Mechanical Strength and Mass Transfer Characteristics. J Chitin Chitosan Sci 2:1–8